ISSN 1330-3651 (Print), ISSN 1848-6339 (Online)

https://doi.org/10.17559/TV-20230202000308
Original scientific paper

Optimization of Rough Self-Propelled Rotary Turning Parameters in terms of Total Energy Consumption and Surface Roughness

An-Le VAN, Trung-Thanh NGUYEN, Xuan-Ba DANG*

Abstract: The self-propelled rotary tool turning (SPRT) process is an economic and effective solution for machining difficult-to-cut materials. This work optimized SPRT parameters, including the inclination angle (*A*), depth of cut (*D*), feed rate (*f*), and turning speed (*V*) to decrease the total energy consumption (*TE*) and surface roughness (*SR*). The turning experiments of the hardened AISI 4150 steel were executed to obtain the experimental data, while the regression method was applied to develop the *TE* and *SR* correlations. The entropy method and quantum-behaved particle swarm optimization (QPSO) were utilized to select the weights and optimal factors. The results indicated that the optimal *A*, *D*, *f*, and *V* were 34 deg., 0.40 mm, 0.47 mm/rev., and 177 m/min, respectively, while the *TE* and *SR* were saved by 9.7% and 35.4%, respectively. The *f* and *V* were found to be the most effective parameters, followed by the *D* and *A*. The outcomes provide valuable data to determine optimal SPRT factors for minimizing energy consumption and maximizing machining quality.The optimizing technique could be applied to solve other issues for different SPRT operations.

Keywords: entropy; process parameters; QPSO; self-propelled rotary tool turning; surface roughness; total energy consumption

1 INTRODUCTION

The SPRT process is an effective approach to increase productivity and machining quality, in which the insert is rotated around itself using friction with the workpiece. The advantages are longer tool life and lower temperature. Consequently, the SPRT can be applied in machining different components [1].

Many attempts have been executed to boost performance measures for various SPRT operations. A simulation model was developed to explore the machining temperature (*MT*) in terms of the *D*, *f*, and *V* [2]. The small errors indicated that the developed model is accurate. A set of experiments of the SPRTAISI 4340 steel using coated inserts was executed [3]. The authors emphasized that the SPRT process provided only the flank wear. A wear model with empirical coefficients of the SPRTAISI 4340 steel was developed [4]. The authors stated that the *V* and *f* had similar impacts on the response. Kishawy et al. presented a new-coated insert to facilitate the SPRT aerospace alloys [5]. The findings revealed that a longer tool life was obtained, while a small insert was recommended to enhance the tool life. The artificial neural network (ANN)-based models of the turning forces were proposed regarding the *V*, *D*, *f*, and *A* [6]. The authors revealed that genetic algorithm-back propagation models could give better accuracy than the conventional back propagation ones. The Oxley analysis-based model was applied to develop the SPRT force models [7]. The results indicated that a high *V* decreased the friction coefficient, while the *f* had the highest contribution to the force. Ezugwu evaluated the machinability of the nickel and titanium base alloys using an efficiently round insert. The author presented that the turning forces and friction on the rake face were lower than the fixed ones [8]. The *SR* and material removal rate (*MRR*) models of the SPRT EN24 steel were developed in terms of the *A*, *D*, *f*, and *V* using the response surface methodology (RSM) [9]. The authors stated that the *SR* was decreased by 14.5% at the same *MRR*. The energy consumption in the turning state (E_t) and *SR* models of the SPRTAISI 4050 steel were developed in terms of the *V*, *A*, *f*, and *D* [10]. The results indicated that the E_t and *SR* were saved by 50.3% and 19.8%, respectively.

The Kriging-based models of the energy efficiency and machining cost of the SPRT hardened steel were developed by Nguyen et al. The authors indicated that the energy efficiency was improved by 8.9% and the machining cost was decreased by 14.8% [11]. A simulation model was applied to forecast the *MT*, cutting forces, chip flow, and induced stresses of the SPRT 51200 steel [12]. The small errors indicated the developed models were reliable. The genetic algorithm was applied to find the optimal values of the *A*, *D*, *f*, and *V* for the SPRTAISI 4140 steel [13]. The authors stated that the *SR* of 0.38 μm, the tool wear of 2.42 μm, and the *MRR* of 11851 mm^3/min could be obtained. Nieslony et al. investigated the impacts of the *V* and *f* on the *SR* and vibration of the SPRT 41Cr4 steel [14]. The outcomes revealed that a higher *V* caused a decreased *SR* and stable machining. Aljinović et al. examined the impacts of the *V*, *f*, and *D* on the *SR* and power consumed (*PC*) of the turning aluminium alloy using the RSM and ANN [15]. The authors stated that the ANN provided a better accuracy for the responses, as compared to the RSM one. The *SR* model of the turning C45 steel was developed in terms of the *A*, radius, rake angle, and approach angle using different regressions [16]. The results indicated that proposed correlations could be applied to precisely predict the roughness value. An optimization was performed to minimize the *PC*, *MT*, and cutting forces of the turning AISI 1045 steel [17]. The authors stated that the optimal *V*, *f*, and *D* were 210 m/min, 0.224 mm/rev, and 1.5 mm, respectively. Vukelic et al. investigated the influences of the *V*, *f*, and *D* on the performance measures for the dry turning Inconel 601 [18]. The results revealed that the dry condition led to acceptable flank wear and roughness, while reductions in energy and machining time were obtained. Sertsoz and Kacal indicated that the *SR* of the MQL turning cast iron was decreased by 37.0%, as compared to the dry condition [19]. Kang et al. explored the vibration amplitudes and frequencies on the *SR* using simulation [20]. The authors revealed that the *SR* was primarily affected by the vibration amplitude.

Leksycki et al. emphasized that higher values of the *V* and *f* increased the intensity of plastic side flow for the dry turning stainless [21]. The predictive models of roughness criteria were developed regarding the *V, f, D*, and noise radius for the hard-turning EN C55 steel [22]. The small errors revealed that the proposed correlations were adequate. The predictive model of the *SR* model was developed regarding the *V*, *f*, *D*, *A*, rake angle, approach angle, and corner radius for the turning AISI 1045 steel [23]. The small deviations indicated that the proposed model was significant. The RSM models of the *SR* and tool wear were developed in terms of the *V*, *f*, and *D* for the dry-turning AISI 1040 steel [24]. The authors stated that the tool wear of 0.15 mm and *SR* of 0.31 μm could be obtained. The GRA and TOPSIS methods were applied to find optimal values of the *V*, *f*, and *D* for minimizing the *SR* and maximizing the *MRR* of the turning S355J2 steel [25]. The results indicated that the optimal *S*, *f*, and *D* were 250 m/min, 0.10 mm/rev, and 1.8 mm, respectively. Trung and Thinh emphasized that the Entropy method and MEREC could be effectively applied to find the optimal *SR* and *MRR* for the turning SK53 steel [26]. Jozić et al. revealed that the MQL and compressed cold air were effective solutions to decrease the *SR* and cutting forces for the tuning EN AW-201, as compared to the MQL and dry conditions [27]. The ANN-based models of the diameter deviations, cylindricity, and *S*R of the dry micro-turning process were developed in terms of the *V*, cutting force, and time. The authors stated that the proposed correlations were adequate and efficiently applied to predict the outputs [28]. The regression models of the *SR*, *MRR*, and cutting forces of the turning AISI 1055 were proposed regarding the *V*, *f*, *D*, and noise radius [29]. The findings indicated the *V* was found to be the most effective factor, followed by the *f*, *D*, and noise radius. Sterpin Valic et al. indicated that the MQL and Ranque-Hilsch vortex were effective approaches to minimize the *SR* and maximize the *MRR* for the turning X20Cr13 steel [30]. However, the limitations of the aforementioned works are expressed as:

The empirical model of the *TE* considering embodied energy footprint of the cutting tool and lubricant has not been presented in the above works.

The selection of optimal factors for simultaneously decreasing the *TE* of *SR* has not been considered.

2 OPTIMIZATION APPROACH
2.1 SPRT Parameters and Responses

The *TE* comprises the energy consumption in the turning cycle (*EC*), the energy footprint for the cutting insert (*ET*), and the energy footprint for the lubricant (*EL*).

$$TE = EC + ET + EL \tag{1}$$

The *EC* comprises the startup (E_s), the standby (E_{st}), transition (E_{ts}), air-turning (E_a), turning (E_t), and tool change (E_{tc}) energy. Therefore, the *EC* model can be expressed as:

$$EC = E_s + E_{st} + E_{ts} + E_a + E_t + +E_{tc} \tag{2}$$

The E_s is computed as:

$$E_s = P_o \times t_o \tag{3}$$

where P_o and t_o are the power and startup time, respectively.

The E_{st} is calculated as:

$$E_{st} = P_{st} \times t_{st} \tag{4}$$

where P_{st} and t_{st} are the power and standby time, respectively.

The E_{ts} is expressed as:

$$E_{ts} = aV^2 + bV + c \tag{5}$$

where *a*, *b*, and *c* present the experimental coefficients.

The E_a is calculated as:

$$\begin{aligned} E_a &= P_a \times t_a = (P_{st} + P_{op}) \times t_a \\ &= (P_{st} + c_1 V + c_2) \times t_a \end{aligned} \tag{6}$$

where P_a denotes the power. c_1 and c_2 are the coefficients of the linear model.

The E_t is calculated as:

$$E_t = P_c \times t_c \tag{7}$$

where P_c and t_c are the power and cutting time, respectively.

The second-order form of the E_t and *SR* models is expressed as:

$$y = \beta_0 + \sum_{i=1}^{k} \beta_i x_i + \sum_{i=1}^{k} \beta_{ii} x_i^2 + \sum_{i=1}^{k} \sum_{j=i+1}^{k} \beta_{ij} x_i x_j + \varepsilon \tag{8}$$

where β_i, β_{ii}, and β_{ij} are the regression coefficients. *k* and *ε* are the number of parameters and error, respectively.

The E_{tc} is computed as:

$$E_{tc} = P_{st} \times t_{tc} \left(\frac{t_c}{T_T}\right) \tag{9}$$

where t_{tc} and T_T are the changing time and tool life, respectively. The T_T is expressed as:

$$T_T = \frac{A}{V^{\alpha} f^{\beta} d^{\gamma}} \tag{10}$$

where *A*, *α*, *β*, and *γ* are the experimental coefficients.

The *ET* is calculated as:

$$ET = \frac{t_c}{T_T} U_m V_{\text{insert}} \tag{11}$$

where U_m and V_{insert} is the energy for fabricating material and volume of one insert, respectively.

The *EL* is computed as:

$$EL = \frac{t_c}{T_L} \times (V_{\text{in}} + V_{\text{ad}})_u \eta \rho E_L \tag{12}$$

where T_L and E_L are the cycle time of the lubricant and energy used to fabricate the lubricant, respectively. V_{in} and V_{ad} are the initial and additional volumes of the lubricant, respectively. ρ and η present the density and concentration of the lubricant, respectively.

The *SR* value is computed as:

$$SR = \sum_{i=1}^{n} \frac{R_{ai}}{n} \tag{13}$$

where R_{ai} is the average roughness at the i^{th} measured point.

Four key factors having the ranges, including the inclination angle, cutting speed, depth of cut, and feed rate are exhibited in Tab. 1. The levels of the cutting speed, depth of cut, and feed rate are selected based on the characteristics of the CNC turning and recommendations of the manufacturer of the round insert. The values of the inclination angle are determined through the configuration of the machine tool. These ranges are confirmed with the related works of the SPRT operations. The optimization issue is expressed as:

Find $X = [A, V, f, \text{and } D]$.

Minimizing *TE* and *SR*;

Constraints: $15 \le A \le 45$ (deg.); $0.4 \le D \le 0.8$ (mm); $0.3 \le f \le 0.7$ (mm/rev.); $80 \le V \le 180$ (m/min).

2.2 Optimization Framework

The optimization procedure is shown in Fig. 1.

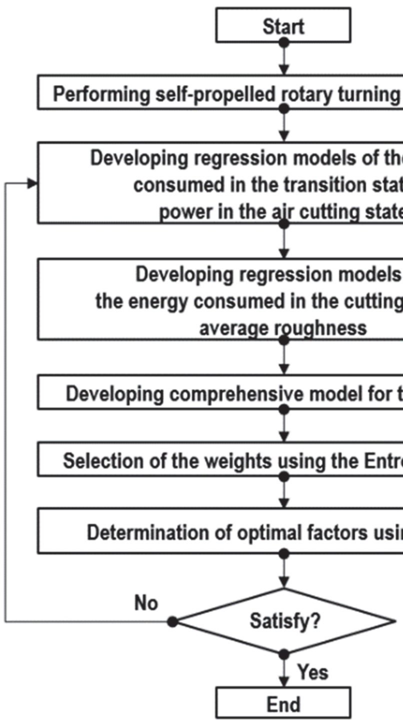

Figure 1 Optimization approach for the SPRT process

- Step 1: Performing turning experiments.
- Step 2: Developing regression models of responses.
- Step 3: Developing the *TE* and *SR* models.
- Step 4: Computing weights of responses.

The normalized response (p_{ij}) is computed as:

$$p_{ij} = \frac{x_{ij}}{\sum_{i=1}^{m} x_{ij}} \tag{14}$$

The entropy value (E_j) is computed as:

$$E_j = -\frac{\sum_{j=1}^{m} p_{ij} \times \ln p_{ij}}{\ln m} \tag{15}$$

The entropy weight (ω_i) is computed as:

$$\omega_i = \frac{1 - E_j}{\sum_{j=1}^{n} (1 - E_j)} \tag{16}$$

Step 5: Selecting optimal data using the QPSO.

To overcome the drawbacks of original PSO, the wave function $\Psi(x, t)$ is applied instead of velocity to enhance the dynamic behavior of the particle. Moreover, probability density function $|\Psi(x, t)|^2$ is utilized to compute the probability distribution of the particle's position. The operating procedure of the QPSO is depicted in Fig. 2.

In the QPSO, the updated position is expressed as:

$$X^j_{i,(t+1)} = P^j_{i,(t+1)} - \beta(M_{\text{best}^j_t} - X^j_{i,t})\ln(\frac{1}{u}) \quad \text{If } k \ge 0.5 \tag{17}$$

$$X^j_{i,(t+1)} = P^j_{i,(t+1)} - \beta(M_{\text{best}^j_t} - X^j_{i,t})\ln(\frac{1}{u}) \quad \text{If } k < 0.5 \tag{18}$$

$$P^j_{i,(t+1)} = \theta P_{\text{best}^j_{i,t}} + (1-\theta) - X^j_{i,t})g_{\text{best}^j_t} \tag{19}$$

$$M_{\text{best}^j_t} = \frac{1}{N}\sum_{i=1}^{N} P_{\text{best}^j_{i,t}} \tag{20}$$

where P_i, P_{best}, g_{best}, and M_{best} are the local attractor, the best positions at the t_{th} iteration, the best position of all particles in the current generation, and the mean best position, respectively. k, u, and θ are random numbers distributed uniformly on [0, 1]. β (contraction expansion coefficient) denotes the tuning parameter to control the convergence speed of the particle and is distributed uniformly on [1, 0.4]. The β value is computed as:

$$\beta = \beta_{\max} - [\frac{\{\beta_{\max} - \beta_{\min}\}}{it_{\max}} it] \tag{21}$$

where $\beta_{\max}$ and $\beta_{\min}$ present the initial expansion and final factors, respectively, while it and $it_{\max}$ are the current iteration and the maximum number of iterations, respectively.

Table 1 Process inputs for the SPRT process

Symbol	Parameters	Values
A	Inclination angle / deg.	15-30-45
D	Depth of cut / mm	0.4-0.6-0.8
f	Feed rate / mm/rev.	0.3-0.5-0.7
V	Turning speed / m/min	80-130-180

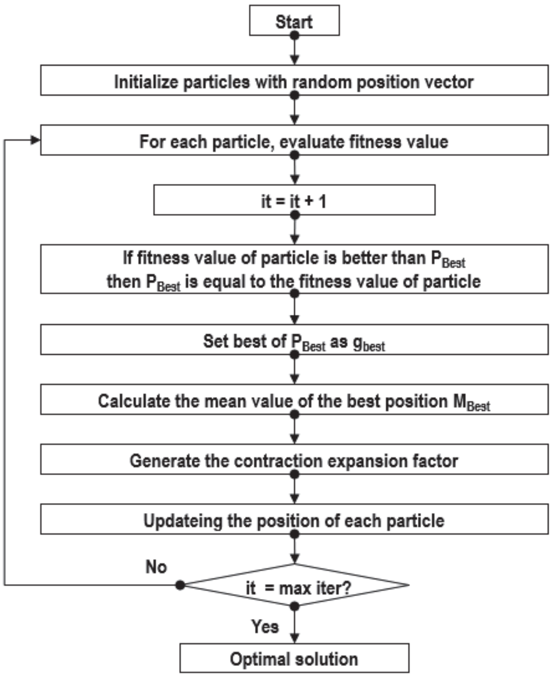

Figure 2 The working principle of the QPSO

3 EXPERIMENTAL SETTING

The round bar with the material entitled AISI 4150 and the hardness of 52 HRC steel is employed as the turning workpiece. Tab. 2 presents the properties of the chosen workpiece. The external diameter and length of each specimen are 40 mm and 300 mm, respectively. The experiments are executed with the support of a CNC lathe entitled EMCOTURN E45 (Fig. 3). The workpiece is tightly clamped using the three jaw chuck and live centre. The hardened steel labeled SKD11 is used to fabricate the tool shank.

Figure 3 SPRT experiments

A power meter entitled KEW6305 produced by KYORITSY using an interval of 0.1 second is utilized to measure the power components. The voltages of 150, 300, and 600 V are employed to operate the device. The reading error of ±0.3% and full-scale error of ±0.2% are applied to minimize the error. The sensor is connected with the electrical source and the machine tool. The turning power is captured and stored in the flashcard. The average value of the power is computed from the 5 highest peaks in the turning duration.

Table 2 The Properties of the AISI 4050

Density	Melting Point	Tensile strength	Yield strength	Elastic modulus	Poisson's ratio	Thermal conductivity
7.85 g/cm^3	1427 °C	731 MPa	380 MPa	210 GPa	0.29	44.5 W/mK

A roughness tester SJ-301 produced by Mitutoyo with ISO 4287 standard is applied. The measured length of 4 mm in the feed direction is used to capture the roughness. The radius diamond of 5 μm is linearly moved on the turned surface. The measured range of 0.05-40 mm and the resolution of 0.01 μm are employed to minimize the error. The average value of the *SR* is computed from 3 positions on the turned surface.

The example results of experiments are shown in Fig. 4.

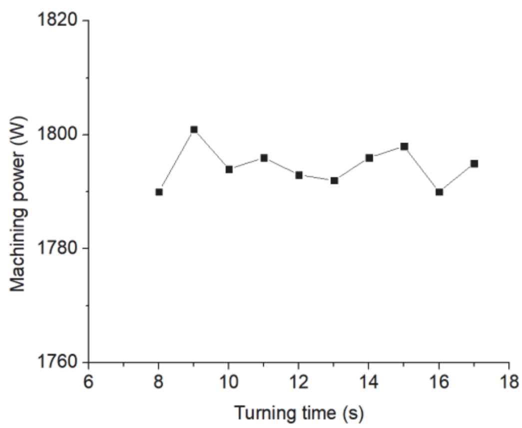

(a) Power consumed at experimental No. 10

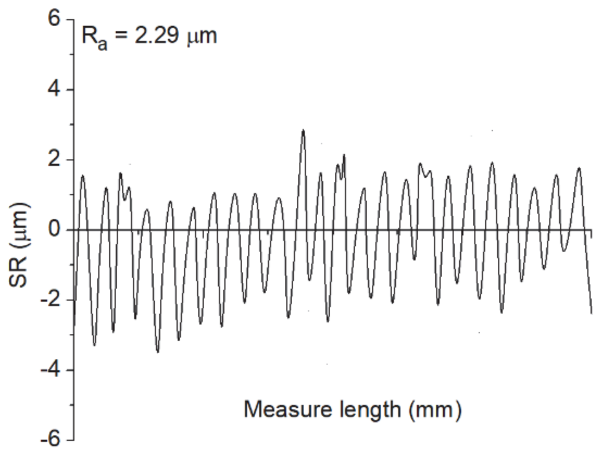

(b) Machined roughness at experimental No. 10

Figure 4 Turning responses at the different process inputs

4 RESULTS AND DISCUSSIONS

4.1 Development of Regression Models

The regression models of the EC_{ts} and P_{op} were shown in Tab. 3. The R^2, *adjusted* R^2, and *predicted* R^2 values indicated that the developed models are adequate.

The experimental data are shown in Tab. 4.

The ANOVA results of the E_t and SR are shown in Tabs. 5 and 6, respectively. The values of the R^2 value, the *adjusted* R^2, and the *predicted* R^2 indicate that the E_t and SR models are adequate.

Table 3 Regression models of the EC_{ts} and P_{op}

Regression model	R^2	*Adj.* R^2	*Pre.* R^2
$EC_{ts} = 0.000025V^2 - 0.0014V + 0.4682$	0.9882	0.9794	0.9654
$P_{op} = 0.0025V + 0.03682$	0.9924	0.9826	0.9758

Table 4 Experimental data for the E_t and SR

No.	A / deg.	D / mm	f / mm/rev.	V / m/min	E_t / kJ	SR / μm
Experimental data for developing regression models						
1	45	0.6	0.5	180	10.63	1.64
2	15	0.4	0.5	130	12.17	1.98
3	30	0.4	0.3	130	16.76	1.17
4	30	0.4	0.7	130	8.91	1.91
5	15	0.6	0.3	130	19.49	1.83
6	30	0.6	0.5	130	12.44	1.76
7	45	0.4	0.5	130	12.56	1.61
8	45	0.6	0.7	130	10.67	2.25
9	30	0.6	0.5	130	12.48	1.77
10	45	0.6	0.5	80	20.34	2.28
11	30	0.8	0.5	80	20.10	2.41
12	30	0.6	0.3	180	15.39	1.24
13	15	0.6	0.7	130	10.28	2.56
14	45	0.6	0.3	130	20.81	1.54
15	30	0.8	0.7	130	10.11	2.44
16	30	0.8	0.5	180	10.33	1.99
17	30	0.6	0.7	80	14.95	2.52
18	30	0.4	0.5	80	16.89	2.03
19	30	0.6	0.7	180	7.43	1.97
20	15	0.6	0.5	80	19.47	2.56
21	15	0.6	0.5	180	10.14	1.94
22	30	0.6	0.3	80	27.51	1.81
23	15	0.8	0.5	130	13.58	2.51
24	30	0.8	0.3	130	19.87	1.86
25	45	0.8	0.5	130	14.25	2.22
26	30	0.4	0.5	180	9.11	1.26
Experimental data for testing developed models						
27	20	0.5	0.4	100	18.41	1.89
28	35	0.7	0.6	120	11.98	2.13
29	40	0.5	0.6	140	9.91	1.76
30	25	0.7	0.4	110	18.29	1.96
31	35	0.6	0.6	130	10.71	1.92
32	40	0.5	0.5	150	11.01	1.52

Table 5 Computed ANOVA results for the E_t

So.	SS	MS	F-value	p-value
Mod	582.0568	41.5755	32.3668	< 0.0001
A	72.6520	72.6520	56.5605	0.0013
D	207.9083	207.9083	161.8593	< 0.0001
f	1010.9443	1010.9443	787.0334	< 0.0001
V	988.5304	988.5304	769.5838	< 0.0001
Af	50.6245	50.6245	39.4118	0.0016
Df	100.8626	100.8626	78.5228	0.0012
DV	104.7270	104.7270	81.5314	0.0011
fV	242.3020	242.3020	188.6353	0.0003
A^2	190.1317	190.1317	148.0200	0.0008
D^2	66.0824	66.0824	51.4460	0.0014
f^2	396.1078	396.1078	308.3751	< 0.0001
V^2	398.8129	398.8129	310.4810	< 0.0001
Re.	14.1296	1.2845		
Total	596.1864			
$R^2 = 0.9763$; *Adj.* $R^2 = 0.9682$; *Pred.* $R^2 = 0.9562$				

For the E_t model, significant factors are single factors (A, D, f, and V), interactive factors (Af, Df, DV, and fV), and quadratic factors (A^2, D^2, f^2, and V^2). The contributions of the A, D, f, and V are 1.88%, 5.38%, 26.16%, and 25.58%, respectively. The contributions of the Af, Df, DV, and fV are 1.31%, 2.61%, 2.71%, and 6.27%, respectively. The contributions of the A^2, D^2, f^2, and V^2 are 4.92%, 1.71%, 10.25%, and 10.32%, respectively.

For the SR model, significant parameters are single factors (A, D, f, and V), interactive factors (AD, Df, and DV), and quadratic factors (A^2, D^2, f^2, and V^2). The contributions of the A, D, f, and V are 9.12%, 17.17%, 20.79%, and 17.68%, respectively. The contributions of the AD, Df, and DV are 1.23%, 2.37%, and 5.19%, respectively. The contributions of the A^2, D^2, f^2, and V^2 are 14.97%, 33.61%, 1.46%%, and 5.54% respectively.

Table 6 Computed ANOVA results for the SR

So.	SS	MS	F-value	p-value
Mod	4.09985	0.29285	35.25623	< 0.0001
A	4.51267	4.51267	543.04083	< 0.0001
D	8.49589	8.49589	1022.36963	< 0.0001
f	10.28710	10.28710	1237.91873	< 0.0001
V	8.74824	8.74824	1052.73704	< 0.0001
AD	0.60862	0.60862	73.23906	0.0006
Df	1.17270	1.17270	141.11916	0.0117
DV	2.56807	2.56807	309.03310	< 0.0001
A^2	7.40731	7.40731	891.37294	< 0.0001
D^2	1.78626	1.78626	214.95366	0.0006
f^2	0.72242	0.72242	86.93417	0.0004
V^2	2.74125	2.74125	329.87349	< 0.0001
Re.	0.09137	0.00831		
Total	4.19122			
$R^2 = 0.9782$; *Adj.* $R^2 = 0.9686$; *Pred.* $R^2 = 0.9654$				

Table 7 Confirmations of the precision of the developed models

No.	E_t / kJ			SR / μm		
	Exp.	Pred.	Err.	Exp.	Pred.	Err.
27	18.41	18.49	–0.43	1.89	1.88	0.53
28	11.98	12.06	–0.67	2.13	2.14	–0.47
29	9.91	9.84	0.71	1.76	1.77	–0.57
30	18.29	18.05	1.31	1.96	1.95	0.51
31	10.71	10.92	–1.96	1.92	1.91	0.52
32	11.01	11.13	–1.09	1.52	1.53	–0.66

The deviations of the Ec and SR change from –1.96% to 1.31% and –0.66% to 0.53%, respectively (Tab. 7), presenting the acceptable accuracy of developed models.

As shown in Fig. 5a, it can be stated that the E_t decreases (relatively around 1.6%) with an increment in the A (from 15 to 25 deg.). A further A (from 25 deg. to 45 deg.), the E_t increased by around 6.5%. A higher A decreases the contact area; hence, the material volume too decreases. The material is softly removed and the E_t decreases. A further A increases the contact area; hence, the material volume increases. The material is hardly turned; hence, the E_t increases.

As shown in Fig. 5b, it can be stated that the E_t increases (relatively around 16.3%) with an increment in the D (from 0.4 to 0.8 mm). A higher D increases the contact area; hence, a higher thickness of the chip is produced. The material is hardly processed; hence, the E_t increases. A higher D increases the machining pressure, resulting in greater resistance. More energy is required to overcome the friction; hence, the E_t increases.

As shown in Fig. 5c, it can be stated that the E_t decreases (relatively around 43.8%) with an increment in the f (from 0.3 to 0.7 mm/rev.). A higher f increases the distance between the successive turning paths; hence, the turning time decreases. The E_t consequently decreases with an increased f.

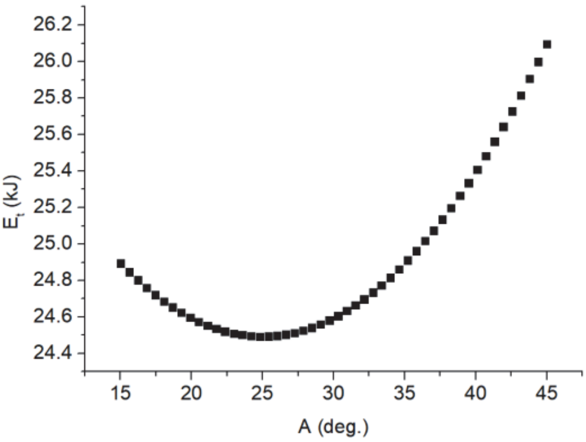

(a) E_t versus A

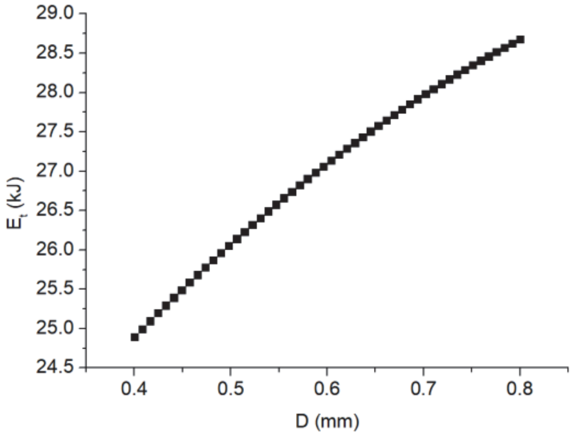

(b) E_t versus *D*

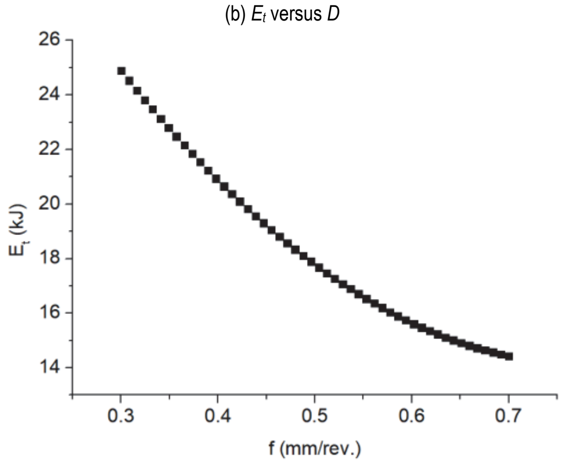

(c) E_t versus *f*

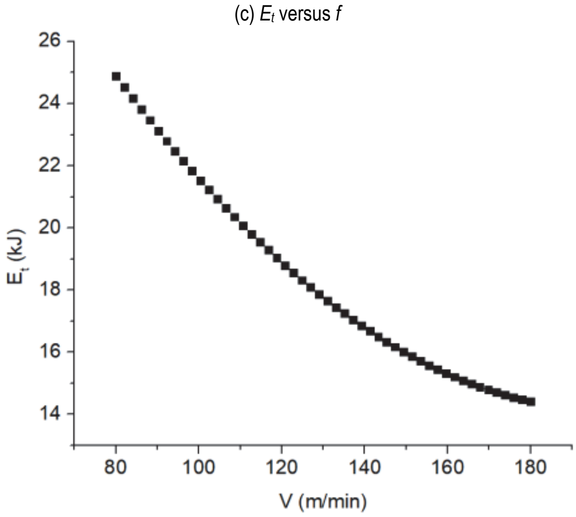

(d) E_t versus *V*

Figure 5 The impacts of process parameters on the E_t

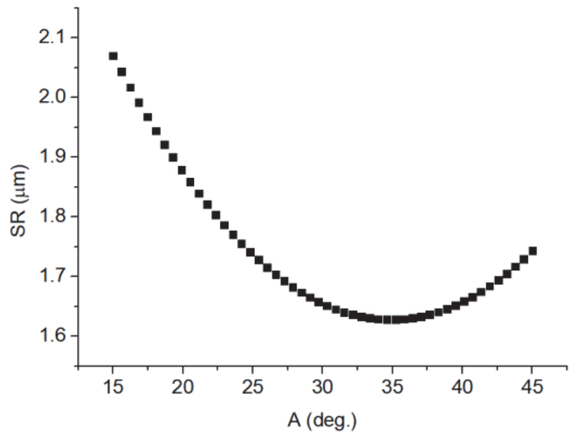

(a) *SR* versus *A*

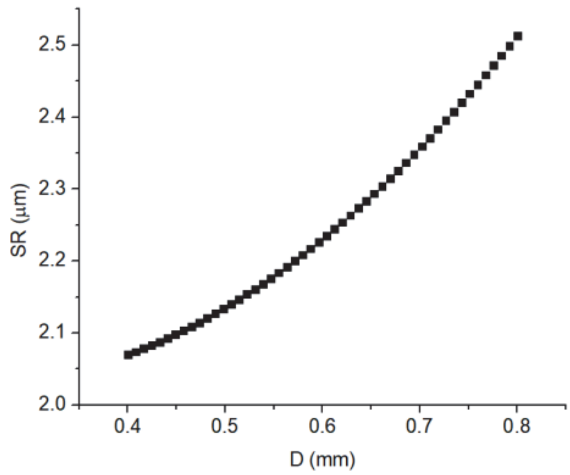

(b) *SR* versus *D*

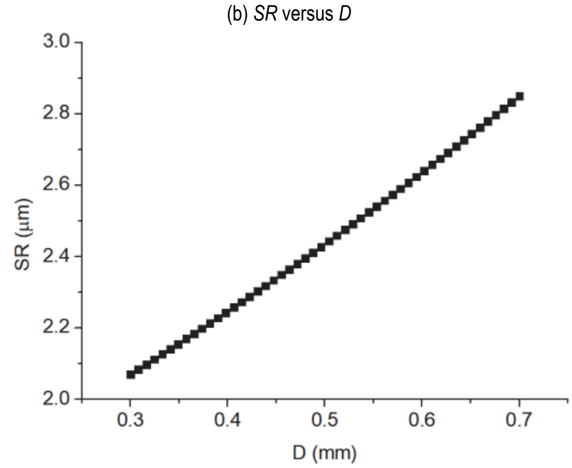

(c) *SR* versus *f*

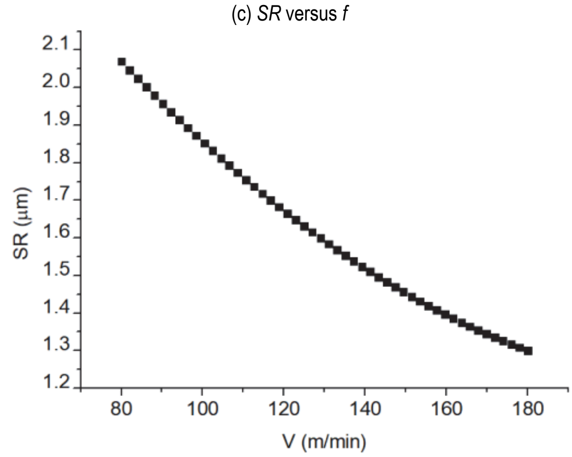

(d) *SR* versus *V*

Figure 6 The impacts of process parameters on the *SR*

As shown in Fig. 5d, it can be stated that the E_t decreases (relatively around 44.2%) with an increment in the V (from 80 to 180 m/min). A higher V increases the machining temperature, leading to reductions in the hardness and strength of the workpiece. The material is easily removed; hence, low energy consumes. A higher f decreases the machining time; hence, the E_t decreases.

As shown in Fig. 6a, it can be stated that the SR decreases (relatively around 23.8%) with an increment in the A (from 15 to 35 deg.). A further A (from 35 deg. to 45 deg.), the SR increased by around 8.6%. A higher A decreases the material volume; hence, the SR decreases. A further A increases the material volume; hence,the SR increases.

As shown in Fig. 6b, the SR increases (relatively around 21.4%) with an increment in the D (from 0.4 to 0.8 mm). A higher D increases the material removal volume; hence, the SR increases. A higher D increases the machining pressure, leading to greater friction; hence, the SR increases.

As shown in Fig. 6c, the SR increases (relatively around 38.1%) with an increment in the f (from 0.3 to 0.7 mm). A higher f increases the feed marks; hence, the SR increases. A higher f causes strain-hardening behavior, leading to unstable machining force; hence, the SR increases.

As shown in Fig. 6d, the SR decreases (relatively around 39.2%) with an increment in the V (from 80 to 180 m/min). A higher V causes an increase in the temperature, leading to reductions in the strength and hardness of the workpiece. The material is softly turned; hence, the SR decreases. A higher V may reduce the vibration, resulting in a stable turning; hence, a low SR is obtained.

The interactions of process parameters on the E_t and SR are shown in Figs. 7 and 8, respectively.

The E_t and SR models are expressed as:

$$E_t = 57.03659 - 0.17639A + 26.11532D - 76.32189f - 0.31401V + 0.023188AD - 0.077016Af - 0.00013AV - 11.96651Df - 0.04974DV \quad (22)$$

$$SR = 3.92708 - 0.07974A - 1.21667D + 1.72042f - 0.02096V + 0.00666AD - 0.00167Af - 0.000006AV - 1.1Df + 0.00875DV + 0.00005fV + 0.00112A^2 + 1.52083D^2 + 0.61458f^2 + 0.00004V^2 \quad (23)$$

4.2 Optimizing Outcomes

Tab. 8 presents the coefficients for computing ADRT responses.

Table 8 Coefficients for the ADRT process

P_o / kW	t_o / s	P_{st} / kW	t_{st} / s	t_a / s	t_{tc} / s	A	α	β
0.48	4	0.72	6	8	8	16.2 × 10^5	2.65	0.27
γ	U_m / kJ/m^3	T_L / month	V_{in} / cm^3	V_{ad} / cm^3	η	ρ / g/cm^3	E_L / J/g	U_m / kJ/m^3
0.37	9.16 × 10^3	1	8.5	4.5	5%	0.92	422984	9.16 × 10^3

The computed values of the TE and SR are presented in Tab. 9. As a result, the weight values of the TE and SR are 0.31 and 0.69, respectively (Tab. 10).

Table 9 The values of *TE* and *SR*

No.	A / deg.	D / mm	f / mm/rev.	V / m/min	TE / kJ	SR / µm
1	15	0.4	0.5	130	27.42	1.98
2	15	0.8	0.5	130	29.25	2.51
3	45	0.4	0.5	130	27.97	1.61
4	45	0.8	0.5	130	30.08	2.22
5	30	0.6	0.3	80	41.29	1.81
6	30	0.6	0.3	180	32.15	1.24
7	30	0.6	0.7	80	29.41	2.52
8	30	0.6	0.7	180	24.86	1.97
9	15	0.6	0.5	80	33.93	2.56
10	15	0.6	0.5	180	27.28	1.94
11	45	0.6	0.5	80	34.81	2.28
12	45	0.6	0.5	180	27.78	1.64
13	30	0.4	0.3	130	32.99	1.17
14	30	0.4	0.7	130	24.36	1.91
15	30	0.8	0.3	130	35.92	1.86
16	30	0.8	0.7	130	25.37	2.44
17	15	0.6	0.3	130	35.09	1.83
18	15	0.6	0.7	130	25.97	2.56
19	45	0.6	0.3	130	36.24	1.54
20	45	0.6	0.7	130	26.19	2.25
21	30	0.4	0.5	80	31.67	2.03
22	30	0.4	0.5	180	25.82	1.26
23	30	0.8	0.5	80	34.64	2.41
24	30	0.8	0.5	180	26.80	1.99
25	30	0.6	0.5	130	28.09	1.76
26	30	0.6	0.5	130	28.04	1.77

The Pareto graph generated by QSPSO is depicted in Fig. 7. It can be stated that SPRT responses have contradictory trends. Lower energy consumption leads to higher surface roughness.

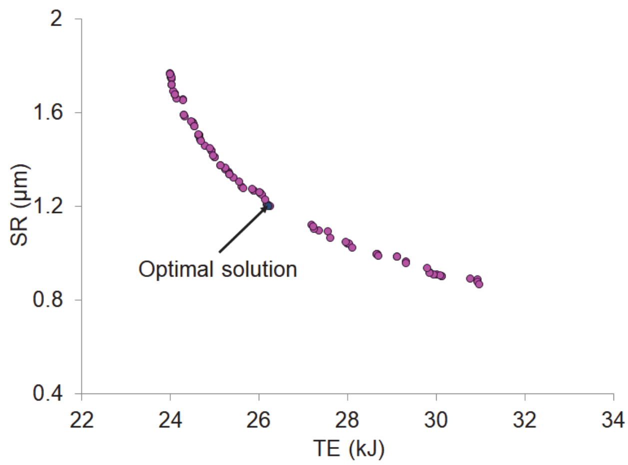

Figure 7 The Pareto front generated by QPSO

Table 10 Entropy value, dispersion value, and weight for *TE* and *SR*

Criteria	TE	SR
Entropy value	0.99700	0.99337
Dispersion value	0.00300	0.00663
Weight	0.31	0.69

As a result, the optimum findings of the A, D, f, and V are 34 deg., 0.40 mm, 0.47 mm/rev., and 177 m/min, respectively. The reductions in the TE and SR are 9.7% and 35.4%, respectively (Tab. 11).

Table 11 Optimization results

Method	*A* deg.	*D* mm	*f* mm/rev.	*V* m/min	*TE* kJ	*SR* μm
Initial values	30	0.40	0.50	100	29.25	1.81
Optimal values	34	0.40	0.47	177	26.17	1.17
Reduction / %					9.7	35.4

5 CONCLUSIONS

In this investigation, the total energy consumption (*TE*) and surface roughness (*SR*) of the SPRT process were decreased using optimal factors, including the inclination angle (*A*), depth of cut (*D*), feed rate (*f*), and turning speed (*V*). The regression method was applied to construct the *TE* and *SR* models, while the QPSO was used to find optimizing data. The conclusions can be expressed as:

For minimizing energy consumption, the low values of the *A* and *D* could be applied, while the high ranges of the *f* and *V* were recommended. For decreasing the surface roughness, the low *D* and *f* were utilized, while the high *A* and *V* could be used.

The *f* and *V* had effective contributions to the *TE* and *SR* models, followed by the *D* and *A*, respectively.

The optimal values of the *A*, *D*, *f*, and *V* were 34 deg., 0.40 mm, 0.47 mm/rev., and 177 m/min, respectively. The *TE* was saved by 9.7% and the *SR* was decreased by 35.4%, as compared to the initial values.

The carbon emissions, machining costs, and noise emissions have not been considered. The impacts of the SPRT parameters on the ecological and economic indicators will be addressed in future works.

6 REFERENCES

[1] Armarego, E. J. A., Karri, V., & Smith, A. J. R. (1994). Fundamental studies of driven and self-propelled rotary tool cutting processes-I. Theoretical Investigation. *International Journal of Machine Tools and Manufacture*, *34*, 785-801. https://doi.org/10.1016/0890-6955(94)90059-0

[2] Dessoly, V., Melkote, S. N., & Lescalier, C. (2004). Modeling and verification of cutting tool temperatures in rotary tool turning of hardened steel. *International Journal of Machine Tools and Manufacture*, *44*, 1463-1470. https://doi.org/10.1016/j.ijmachtools.2004.05.007

[3] Kishawy, H. A. & Wilcox, J. (2003). Tool wear and chip formation during hard turning with self-propelled rotary tools. *International Journal of Machine Tools and Manufacture*, *43*, 433-439. https://doi.org/10.1016/S0890-6955(02)00239-0

[4] Kishawy, H. A., Pang, L., & Balazinski, M. (2011). Modeling of tool wear during hard turning with self-propelled rotary tools. *International Journal of Mechanical Sciences*, *53*, 1015-1021. https://doi.org/10.1016/j.ijmecsci.2011.08.009

[5] Kishawy, H. A., Becze, C. E., & McIntosh, D. G. (2004). Tool performance and attainable surface quality during the machining of aerospace alloys using self-propelled rotary tools. *Journal of Materials Processing Technology*, *152*, 266-271. https://doi.org/10.1016/j.jmatprotec.2003.11.011

[6] Wang, S. H., Zhu, X., Li, X., & Turyagyenda, G. (2006). Prediction of cutting force for self-propelled rotary tool using artificial neural networks. *Journal of Materials Processing Technology*, *180*, 23-29. https://doi.org/10.1016/j.jmatprotec.2006.04.123

[7] Li, L. & Kishawy, H. A. (2006). A model for cutting forces generated during machining with self-propelled rotary tools. *Journal of Materials Processing Technology*, 46, 1388-1394. https://doi.org/10.1016/j.ijmachtools.2005.10.003

[8] Ezugwu, E. O. (2007). Improvements in the machining of aero-engine alloys using self-propelled rotary tooling technique. *Journal of Materials Processing Technology*, *185*, 60-71. https://doi.org/10.1016/j.jmatprotec.2006.03.112

[9] Rao, T. B., Krishna, A. G., Katta, R. K., & Krishna, K. R. (2015). Modeling and multi-response optimization of machining performance while turning hardened steel with self-propelled rotary tool. *Advances in Manufacturing*, *3*, 84-95. https://doi.org/10.1007/s40436-014-0092-z

[10] Nguyen, T. T. (2020). An energy-efficient optimization of the hard turning using rotary tool. *Neural Computing and Application*, *33*, 2621-2644. https://doi.org/10.1007/s00521-020-05149-2

[11] Nguyen, T. T., Duong, Q. D., & Mia, M. (2020). Sustainability-based optimization of the rotary turning of the hardened steel. *Metals*, *10*, 939. https://doi.org/10.3390/met10070939

[12] Umer, U., Kishawy, H., Abidi, M. H., Mian, S. H., & Moiduddin, K. (2020). Evaluation of self-propelled rotary tool in the machining of hardened steel using finite element models. *Materials*, *13*, 5092. https://doi.org/10.3390/ma13225092

[13] Ahmed, W., Hegab, H., Mohany, A., & Kishawy, H. (2021) Analysis and optimization of machining hardened steel aisi 4140 with self-propelled rotary tools. *Materials*, 14, 6106. https://doi.org/10.3390/ma14206106

[14] Nieslony, P., Krolczyk, G., Chudy, R., Wojciechowski, S., Maruda, R., Biłous, P., Lipowczyk, M., & Stachowiak, L. Study on physical and technological effects of precise turning with self-propelled rotary tool. *Precision Engineering*, *66*, 62-75. https://doi.org/10.1016/j.precisioneng.2020.06.003

[15] Aljinović, A., Bilić, B., Gjeldum, N., & Mladineo, M. (2021). Prediction of surface roughness and power in turning process using response surface method and ANN. *Tehnički vjesnik*, *28*(2), 456-464. https://doi.org/10.17559/TV-20190522104029

[16] Vukelic, D., Simunovic, K., Kanovic, Z., Saric, T., Doroslovacki, K., Prica, M., & Simunovic, G. (2022). Modelling surface roughness in finish turning as a function of cutting tool geometry using the response surface method, Gaussian process regression and decision tree regression. *Advances in Production Engineering & Management*, *17*(3), 367-380. https://doi.org/10.14743/apem2022.3.442

[17] Sredanovic, B., Cica, D., Borojevic, S., Tesic, S., & Kramar, D. (2022). Multi-objective optimization of sustainable steel aisi 1045 turning energy parameters under mql condition. *Tribology in Industry*, *44*(3), 498-507. https://doi.org/10.24874/ti.1301.05.22.07

[18] Vukelic, D., Simunovic, K., Simunovic, G., Saric, T., Kanovic, Z., Budak, I., & Agarski, B. (2020). Evaluation of an environment-friendly turning process of Inconel 601 in dry conditions. *Journal of Cleaner Production*, *266*, 121919. https://doi.org/10.1016/j.jclepro.2020.121919

[19] Sertsoz, S. & Kacal, A. (2021) Nano MoS2 application in turning process with minimum quantity lubrication technique (MQL). *Tehnicki vjesnik - Technical Gazette*, *28*(1), 70-76. https://doi.org/10.17559/tv-20190820115047

[20] Kang, W. T., Derani, M. N., & Ratnam, M. M. (2020). Effect of Vibration on Surface Roughness in Finish Turning: Simulation Study. *International Journal of Simulation Modelling*, *19*(4), 595-606. https://doi.org/10.2507/ijsimm19-4-531

[21] Leksycki, K., Feldshtein, E., & Ociepa, M. (2021). On the effect of the side flow of 316l stainless steel in the finish

turning process under dry conditions. *Facta Universitatis, Series: Mechanical Engineering*, *19*(2), 335. https://doi.org/ 10.22190/fume191118019l

[22] Tomov, M., Gecevska, V., & Vasileska, E. (2022). Modelling of multiple surface roughness parameters during hard turning: A comparative study between the kinematical-geometrical copying approach and the design of experiments method (DOE). *Advances in Production Engineering Management*, *17*(1), 75-88. https://doi.org/10.14743/apem2022.1.422

[23] Vukelic, D., Prica, M., Ivanov, V., Jovicic, G., Budak, I., & Luzanin, O. (2022). Optimization of surface roughness based on turning parameters and insert geometry. *International Journal of Simulation Modelling*, *21*(3), 417-428. https://doi.org/10.2507/ijsimm21-3-607

[24] Vukelic, D., Simunovic, K., Kanovic, Z., Saric, T., Tadic, B., & Simunovic, G. (2021). Multi-objective optimization of steel AISI 1040 dry turning using genetic algorithm. *Neural Computing and Applications*, *33*(9), 12445-12475. https://doi.org/10.1007/s00521-021-05877-z

[25] Ficko, M., Begic-Hajdarevic, D., Hadziabdic, V., & Klancnik, S. (2020). Multi-response optimisation of turning process parameters with GRA and TOPSIS methods. *International Journal of Simulation Modelling*, *19*(4), 547-558. https://doi.org/10.2507/ijsimm19-4-524

[26] Trung, D. D. & Thinh, H. X. (2021). A multi-criteria decision-making in turning process using the MAIRCA, EAMR, MARCOS and TOPSIS methods: A comparative study. *Advances in Production Engineering & Management*, *16*(4), 443-456. https://doi.org/10.14743/apem2021.4.412

[27] Jozić, S., Dumanić, I., & Bajić, D. (2020). Experimental analysis and optimization of the controllable parameters in turning of EN AW-2011 alloy; dry machining and alternative cooling techniques. *Facta Universitatis, Series: Mechanical Engineering*, *18*(1), 013. https://doi.org/10.22190/fume191024009j

[28] Vukelic, D., Kanovic, Z., Sokac, M., Santosi, Z., Budak, I. & Tadic, B. (2021). Modelling of micro-turning process based on constant cutting force. *International Journal of Simulation Modelling*, *20*(1), 146-157. https://doi.org/10.2507/ijsimm20-1-553

[29] Nguyen Hong, S. & Vo Thi Nhu, U. (2021). Multi-objective optimization in turning operation of AISI 1055 steel usingDEAR method. *Tribology in Industry*, *43*(1), 57-65. https://doi.org/10.24874/ti.1006.11.20.01

[30] Sterpin Valic, G., Cukor, G., Jurkovic, Z., & Brezocnik, M. (2019). Multi-criteria optimization of turning of martensitic stainless steel for sustainability. *International Journal of Simulation Modelling*, *18*(4), 632-642. https://doi.org/10.2507/ijsimm18(4)495

Contact information:

An-Le VAN
Faculty of Engineering and Technology,
Nguyen Tat Thanh University,
300A Nguyen Tat Thanh Street, Ward 13, District 4,
Ho Chi Minh City 70000, Vietnam
E-mail: lvan@ntt.edu.vn

Trung-Thanh NGUYEN
Faculty of Mechanical Engineering,
Le Quy Don Technical University,
236 Hoang Quoc Viet, Ha Noi 100000, Vietnam
E-mail: trungthanhnguyen@lqdtu.edu.vn

Xuan-Ba DANG
(Corresponding author)
Department of Automatic Control,
Ho Chi Minh City University of Technology and Education,
No. 1 Vo Van Ngan Street, Linh Chieu Ward, Thu Duc City,
Ho Chi Minh City 70000, Vietnam
E-mail: badx@hcmute.edu.vn